

# Dynamics analysis on cavitation flow field of centrifugal pumps using modal order reduction

Yancheng ZHANG<sup>1</sup>, Lei ZHANG<sup>2</sup>, Cong WANG<sup>1</sup>, Tengjiao SUN<sup>2</sup>, Z. LI<sup>3</sup>, and Dezhi JIANG<sup>1</sup> 

<sup>1</sup> College of Engineering, Ocean University of China, Qingdao, 266100, China

<sup>2</sup> Qingdao Port Ferry & Barge Co., Ltd, Qingdao, 266011, China

<sup>3</sup> Faculty of Mechanical Engineering, Opole University of Technology, 45-758 Opole, Poland

**Abstract.** Throughout the operational lifecycle of centrifugal pumps, cavitation is an omnipresent phenomenon that frequently leads to cavitation erosion and a decline in hydraulic heads, leading to mechanical failures and substantial damage to the pump assembly. Although the cavitation phenomenon has been widely studied in existing literature, it is still a challenging task for reliable flow dynamics analysis of centrifugal pumps using the modal order reduction technique. In this study, the modal decomposition and reconstruction of the flow field of a centrifugal pump considering the cavitation are conducted. The dynamic modal decomposition (DMD) based on the singular value decomposition (SVD) is employed to explore the dynamic behaviour of the cavitation flow field by reducing the modal order of the flow field. Then, the modal characteristics of the pump flow field are systematically analyzed. The results demonstrate that the DMD method can improve the accuracy of the order reduction model and reduce the modal reconstruction error, the reconstruction error loss is less than 5%, and the calculation efficiency is significantly enhanced to analyze the pump cavitation flow field. In addition, a comparison of the calculation data between the finite element simulation and the DMD reconstructed flow field indicates the potential application of the DMD method in investigating the degradation of the flow field due to cavitation, which provides new perspective and solid technique support for centrifugal pump cavitation analysis.

**Keywords:** centrifugal pump; cavitation flow field; modal analysis; dynamic modal decomposition.

## 1. INTRODUCTION

Centrifugal pumps, as typical rotating fluid machinery, have been widely used in various ships and warships because of their compact structure and small size level. In ship machinery and equipment, the pump equipment accounts for 15%-30%, of which more than 70% are centrifugal pumps. In the operation process of the centrifugal pumps, cavitation is often found in the flow field. The cavitation is a phenomenon in which vapour bubbles or air bubbles in a liquid are formed at pressures lower than the saturation vapor pressure [1, 2]. When the fluid flows through the impeller of a centrifugal pump, cavitation occurs if the pressure in some areas drops, noted as in the “vapor core theory” [3]. Accordingly, if air bubbles exist in the liquid, the growth of bubbles will lead to cavitation [4]. The occurrence of cavitation will destroy the conveying media continuity of the centrifugal pump, resulting in the efficiency drop of the centrifugal pumps and generating noise and wheezing [5, 6]. In addition, air bubbles will collapse when transported to the high-pressure region, releasing shock waves and micro-jets to permanently damage the surfaces of the pump components [7, 8]. As a result, it is essential to analyze the cavitation of the centrifugal pump flow field to improve the anti-cavitation performance and stability of the centrifugal pumps.

Due to the limitations of objective experimental conditions, computational fluid dynamics (CFD) is a suitable tool for numerical calculations on the cavitation of centrifugal pumps [9–11]. Many difficult-to-observe cavitation can be analyzed using the CFD simulation [12]. Hirschi *et al.* [13] predicted the performance degradation of the centrifugal pumps by comparing the cavitation simulation and with model testing results considering the effect of the diffusers on the performance of the pumps in the cavitation flow. Li *et al.* [14] used the CFD simulation and experimental verification to investigate the cavitation phenomenon of liquid-gas two-phase flow inside the centrifugal pump to optimize the impeller structural parameters. Although the CFD is useful for centrifugal pump simulation, a proper meshing number for the CFD model is needed to determine the size of the calculation domain and to obtain more detailed flow field information. The increase in the meshing number will inevitably increase the requirements on computer performance, including processing power and memory capacity, which will lead to a significant increase in computation time in the flow field simulation. Moreover, the CFD mainly describes the macroscopic level of the flow field, while the microscopic study of the flow field still needs to be improved. To shorten the computation time and reduce the solution dimension of the simulation model, the dynamic mode decomposition (DMD) method based on the singular value decomposition (SVD) is employed in this study to conduct an in-depth analysis of the characterization of the cavitation flow field in the centrifugal pumps with the purpose of rapid downscaling the flow field.

\*e-mail: jdz@ouc.edu.cn

Manuscript submitted 2024-08-12, revised 2025-02-18, initially accepted for publication 2025-04-14, published in July 2025.

Currently, two typical modal decomposition methods are the proper orthogonal decomposition (POD) and the DMD, both are data-driven algorithms. The original DMD was proposed by Professor Schmid [15, 16] based on the decomposition of Koopman's complex system, where the time-resolved data snapshots are processed by an iterative Krylov technique to extract the dynamic flow features and decompose the data into dynamic patterns. The DMD has been applied to the orifice plate jets [17], open cavity flow [18], wake flow [19], and wave packets [20]. The DMD not only realizes the decomposition and reconstruction of the flow field but also obtains the dominant-frequency modal features [21, 22]. Zhi *et al.* [23] applied the DMD method to the decomposition and reconstruction of the wake modes of a ship propeller under light-loaded conditions. They derived the results based on the DMD degradation model for the flow field reconstruction and prediction of the feasible propeller wake. For the identification of the centrifugal pump cavitation and characterization of the pump flow field, Liu *et al.* [24] investigated the effect of different cavitation modes on the vibration amplitude of the flexible hydrofoils with the fluid-solid coupling effect based on the DMD and POD. Liu *et al.* [25] employed the DMD method to perform the dynamic modal decomposition and reconstruct a helical axial multiphase pump, revealing the primary frequencies and corresponding coherent structures within the multiphase pump. Han and Tan [26] used the DMD method to decompose and reconstruct the leakage vortex at the top of the impeller inside a mixed-flow pump. Although there is a growing depth of theoretical research on the DMD by the aforementioned researchers, very limited work has been done to address the DMD-tailored analysis for the centrifugal pumps with concerning the cavitation flow fields. The cavitation flow fields induced by the centrifugal pumps exhibit a high degree of complexity, and the modal decomposition of these flow fields is still inadequately explored.

To bridge this research gap, an improved DMD method based on the SVD is proposed in this study to analyze the characteristics of the cavitation flow field in centrifugal pumps. The aim is to gain a deeper understanding of the gas-liquid flow properties within the centrifugal pumps, thereby enabling a more accurate analysis of the flow field under the cavitation conditions. The analysis results indicate that the proposed DMD method is valuable for rapid order reduction, modal decomposition, and reconstruction of the cavitation flow fields, and hence, plays a critical role in identifying the cavitation and preventing cavitation erosion to avoid pump failures.

## 2. DYNAMICS MODELLING

The DMD originated in fluid dynamics and allows for decomposing complex flow fields into simple representations in space and time domains. The DMD arranges the raw data collected from experiments or simulations into the vector form of consecutive snapshots according to the chronological order in the following form:

$$X_1^N = [x_1, x_2, x_3, \dots, x_i, \dots, x_N], \quad (1)$$

where  $x_i$  is the flow field data snapshot at the  $i$ -th moment, and  $N$  is the total number of data snapshots. If the flow field data is linearly related, there will exist a constant linear mapping  $A$  that connects the snapshot  $x_i$  with the next snapshot, i.e.,

$$x_{i+1} = Ax_i. \quad (2)$$

Two snapshot matrices can be constructed using the snapshots of the flow field from 1 to  $N$  moments. Based on the assumptions of equation (2), it can be obtained that

$$\begin{aligned} Y_2^N &= [x_2, x_3, x_4, \dots, x_N] \\ &= [Ax_1, Ax_2, Ax_3, \dots, Ax_{N-1}] = AX_1^{N-1}. \end{aligned} \quad (3)$$

Based on the linear assumptions, one can derive

$$X_1^N = [x_1, Ax_1, A^2x_1, \dots, A^{i-1}x_1, \dots, A^{N-1}x_1]. \quad (4)$$

Compose the snapshot  $x_n$  with the previous  $n-1$  snapshots into a linear combination, i.e.,

$$x_N = c_1x_1 + c_2x_2 + c_3x_3 + \dots + c_{N-1}x_{N-1} + r, \quad (5)$$

where  $c_1, c_2, c_3, \dots, c_{N-1}$  are the linear coefficients and  $r$  is the residual vector. According to equations (2) and (5) we can obtain

$$AX_1^{N-1} = Y_2^N = X_1^{N-1}S + re_{N-1}^T, \quad (6)$$

where  $S$  can be expressed as

$$S = \begin{bmatrix} 0 & & & c_1 \\ 1 & 0 & & c_2 \\ & \cdot & \cdot & \cdot \\ & & 1 & 0 & c_{N-2} \\ & & & 1 & c_{N-1} \end{bmatrix}. \quad (7)$$

Equations (1)–(7) present the transformation of the unitary matrix. For accurate extraction of the multistep modes in the flow field, the snapshots are particularly important in the presence of noise or uncertainties. Meanwhile, to improve the robustness of the DMD, an improved DMD based on the SVD is proposed. By performing the SVD decomposition to the raw data, it yields

$$X_1^{N-1} = U\Sigma V^H, \quad (8)$$

$$A = U\tilde{A}U^H, \quad (9)$$

where  $\Sigma$  is a diagonal matrix, and the diagonal elements contain  $r$  singular values. In the SVD process, we can keep only  $r$  major singular values and truncate the rest of the small singular values to reduce the numerical noise. The unitary matrices  $U$  and  $V$  obtained from the SVD satisfy  $U^H U = I'$  and  $V^H V = I$ . The process of computing the matrix  $A$  can be regarded as a minimization problem of the Frobenius paradigm

$$\underset{A}{\text{minimize}} \|Y_2^N - AX_1^{N-1}\|_F^2. \quad (10)$$

According to equations (8) and (9), equation (10) can be rewritten as

$$\underset{\tilde{A}}{\text{minimize}} \|Y - U\tilde{A}\Sigma V^H\|. \quad (11)$$

The matrix  $A$  can be approximated by

$$A \approx \tilde{A} = U^H Y V \Sigma^{-1}. \quad (12)$$

Since  $\tilde{A}$  is a similar transformation of  $A$ , matrix  $\tilde{A}$  contains the main eigenvalues of  $A$ . Remember that the  $i$ -th eigenvalue of  $\tilde{A}$  is  $\mu_i$  and the  $i$ -th eigenvector is  $w_i$ . Then, the  $i$ -th DMD modality can be obtained as

$$\mu_i = U w_i. \quad (13)$$

Let the column vector of the eigenvectors  $w_i$  be  $W$ . The eigen decomposition of  $\tilde{A}$  can be expressed as

$$\tilde{A} = W N W^{-1}, \quad N = \text{diag}(\mu_1, \dots, \mu_r) \quad (14)$$

where  $N$  is the diagonal array of the singular values. The snapshot of the flow field at an arbitrary moment can be obtained as

$$\begin{aligned} x_i &= A x_{i-1} = U \tilde{A} U^H x_{i-1} \\ &= U W N W^{-1} U^H x_{i-1} = U W N^{i-1} W^{-1} U^H x_1. \end{aligned} \quad (15)$$

Each column defining  $\Phi$  is a DMD mode, which is obtained according to equation (13)

$$\Phi = U W, \quad (16)$$

$$\alpha = W^{-1} z_1 = W^{-1} U^H x_1, \quad \alpha = [\alpha_1, \dots, \alpha_r]^T, \quad (17)$$

where  $\alpha$  is the mode amplitude and  $\alpha_i$  is the  $i$ -th mode amplitude, which represents the mode contribution to the initial snapshot  $x_1$ . Substituting equations (16) and (17) into equation (15), it yields the predicted flow field at arbitrary moment as

$$x_i = \Phi \Lambda^{i-1} \alpha = \sum_{i=1}^r \Phi_i (\mu_i)^{i-1} \alpha_i, \quad (18)$$

where  $r$  denotes the number of main eigenvalues of  $A$ . Thus, a sequence of snapshots  $X_1^{N-1}$  can be obtained as

$$\begin{aligned} [x_1, x_2, \dots, x_{N-1}]_{X^{N-1}} &= [\varphi_1, \varphi_2, \dots, \varphi_{N-1}]_{\Phi} \begin{bmatrix} \alpha_1 \\ \alpha_2 \\ \dots \\ \alpha_{N-1} \end{bmatrix} \\ &= \begin{bmatrix} 1 & \mu_1 & \dots & \mu_1^{N-1} \\ 1 & \mu_2 & \dots & \mu_2^{N-1} \\ \vdots & \vdots & \vdots & \vdots \\ 1 & \mu_{N-1} & \dots & \mu_{N-1}^{N-1} \end{bmatrix}_{V_{\text{and}}} \cdot \alpha \end{aligned} \quad (19)$$

where the evolution of the flow field is realized by the Vandermonde matrix of  $V_{\text{and}}$ .

### 3. REDUCED ORDER MODELLING

#### 3.1. Physical model

The cavitation significantly influences the performance of the centrifugal pumps. In this study, the IS-65-50-160 centrifugal pump is taken as the research object, and its cavitation is studied using the proposed DMD. Table 1 shows the basic design parameters of the IS-65-50-160 centrifugal pump.

**Table 1**

Basic design parameters of IS-65-50-160 centrifugal pump

Parameters	Symbol	Values	Units
Rated flow rate	$Q_d$	25	m <sup>3</sup> /h
Rated head	$H_d$	32	m
Nominal rotating speed	$n$	2900	rpm
Inlet diameter	$D_{\text{in}}$	65	mm
Outlet diameter	$D_{\text{out}}$	50	mm
Impeller diameter	$D_{\text{imp}}$	160	mm
Blade number	$Z$	5	

In three-dimensional (3D) modelling of the centrifugal pump, the core components include the entire system impeller, worm casing, and the inlet and outlet sections. The geometric modelling is performed in Solidworks according to the dimensions and geometric processing of the computational domain modelling. Figure 1 shows the computational domain of the centrifugal pump.

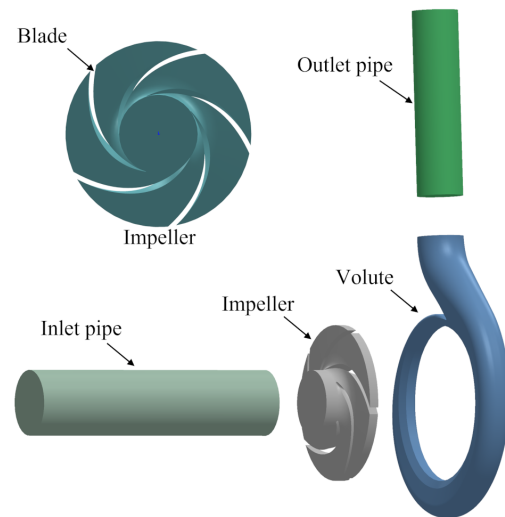


**Fig. 1.** Calculation domain of centrifugal pump

#### 3.2. Mesh segmentation and model validation

The geometric model constructed in Solidworks is imported into the ICEM software to mesh the computational domain. The hexahedral structured mesh is used because the inlet and outlet sections belong to the cylindrical shape. The shapes of the worm shell and impeller are curved and irregular and their structures are more complicated, so the hexahedral structured mesh is not suitable for meshing them. Because the unstructured

meshes can flexibly adapt to complex and irregular geometries to capture complex boundaries and internal details, it is suitable to use the unstructured meshes for the fluid flow. Therefore, the unstructured meshes are used for meshing the worm casing and impeller. The mesh files for each component of the centrifugal pump are generated sequentially, as shown in Fig. 2.

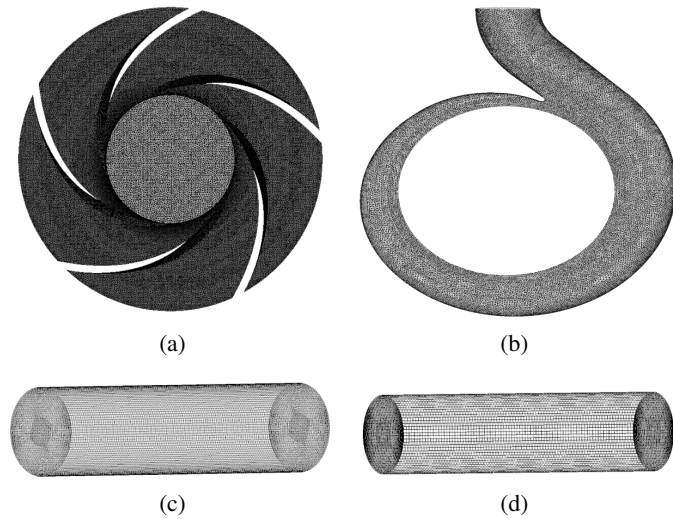


**Fig. 2.** Mesh of the calculation domain: (a) impellers; (b) volute; (c) inlet pipe; (d) outlet pipe

The numerical simulations are performed using fluent commercial software. In the simulation, the number and quality of the meshes have an important impact on the computational structure, and the mesh-independence test can ensure the accuracy and reliability of the computational results. By comparing the computational results under different grid densities, one can confirm the mesh number and quality of the grid division do not affect the calculation results. In addition, the mesh-independence test can verify the stability of the numerical model and identify sensitive areas for local encryption, thus improving the overall computational accuracy. To check the mesh independence, the centrifugal pump model is divided into six groups with different numbers of mesh. Figure 3 shows the mesh-independence test results.

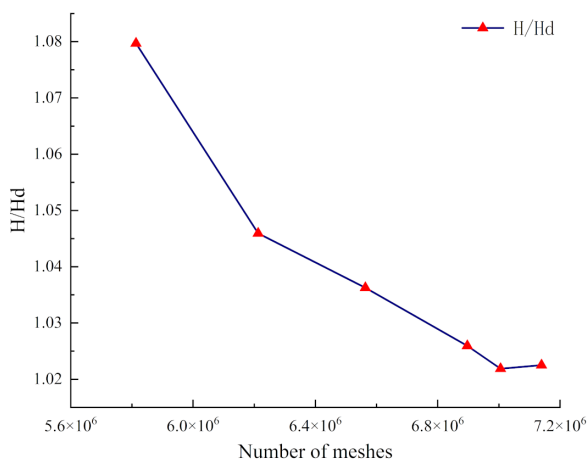


**Fig. 3.** Independence test of mesh elements

From Fig. 3 it can be seen that when the mesh number is around 7 million, the centrifugal pump model exhibits a little change. Considering the computational efficiency and computation time, the mesh number of 7 005 636 in the fifth group is finally selected in this study. The mesh number of each component is shown in Table 2.

**Table 2**

Mesh number in the computational domain

Mesh group	Inlet pipe	Impellers	Volute	Outlet pipe	Number of meshes
1	528 624	4 056 231	982 359	246 358	5 813 572
2	573 296	4 277 269	1 097 562	264 891	6 213 018
3	590 338	4 513 435	1 183 665	275 860	6 563 298
4	596 512	4 746 552	1 268 449	285 440	6 896 953
5	596 512	4 825 057	1 298 627	285 440	7 005 636
6	596 512	4 953 214	1 304 426	285 440	7 139 592

### 3.3. Turbulence model

Wang *et al.* [27] and Wu *et al.* [28] found that the large-eddy simulation (LES) turbulence model provides superior simulation accuracy and a more detailed representation of the flow field characteristics compared to the  $k-\varepsilon$  turbulence model. However, the LES model comes with a significant computational cost, as it requires finer grids to resolve large-scale vortices, which in turn increases the demand for computational resources and time. On the other hand, Yamamoto and Tsujimoto [29] suggested that the  $k-\varepsilon$  turbulence model, while less computationally expensive, is still capable of reasonably predicting the vortex structure. Given its efficiency in terms of computational resources, the standard  $k-\varepsilon$  model is often preferred. In the  $k-\varepsilon$  model, the turbulence viscosity coefficient  $C_\mu$  is solved by the two parameters of  $k$  and  $\varepsilon$ , as expressed in equation (20)

$$\mu_1 = \rho C_\mu \frac{k^2}{\varepsilon}, \quad (20)$$

where  $C_\mu$  is the viscosity coefficient,  $k$  is the turbulent kinetic energy, and  $\varepsilon$  is the turbulent dissipation rate. The turbulent kinetic energy  $k$  and its dissipation rate are obtained from the following transport equations:

$$\frac{\partial(\rho k)}{\partial t} + \frac{\partial(\rho k u_i)}{\partial x_i} = \frac{\partial}{\partial x_j} \left[ \left( \mu + \frac{\mu_t}{\sigma_k} \right) \frac{\partial k}{\partial x_j} \right] + G_k + G_b - \rho \varepsilon - Y_M + S_k, \quad (21)$$

$$\frac{\partial(\rho \varepsilon)}{\partial t} + \frac{\partial(\rho \varepsilon u_i)}{\partial x_i} = \frac{\partial}{\partial x_j} \left[ \left( \mu + \frac{\mu_t}{\sigma_\varepsilon} \right) \frac{\partial \varepsilon}{\partial x_j} \right] + C_{1\varepsilon} \frac{\varepsilon}{k} (G_k + C_{3\varepsilon} G_b) - C_{2\varepsilon} \rho \frac{\varepsilon^2}{k} + S_\varepsilon, \quad (22)$$

where the constants are generally defined as  $C_{1\varepsilon} = 1.44$ ,  $C_{2\varepsilon} = 1.92$ ,  $C_\mu = 0.09$ ,  $\sigma_k = 1.0$ , and  $\sigma_\varepsilon = 1.3$ .

### 3.4. Initial conditions

The boundary conditions are set in the fluent using the total pressure inlet and the mass flow outlet; the impeller region in the computational domain takes the rotational coordinate system, the rest of the region adopts the refined coordinate system, and the residual convergence accuracy is  $10^{-4}$ ; the wall surface uses the no-slip wall surface. The operating medium of the centrifugal pump is water, the saturated vapor pressure of water is set to 3167 Pa, the volume fraction of vacuoles at the inlet is 0, and the volume fraction of water is 1. The time step is recorded once using  $5^\circ$  rotation of the impeller, and the time interval  $dt = 2.78 \cdot 10^{-4}$  s at a rated speed of 2900 rpm.

## 4. RESULTS AND DISCUSSION

Numerical simulation is carried out using the proposed DMD method to analyze the flow field of the pump model, and the degree of the pump cavitation is varied by changing the inlet pressure. For engineering applications, a 3% decrease in the centrifugal pump head usually means cavitation [30]. Define the cavitation number  $\sigma$  to indicate the severity of the occurrence of the cavitation. A smaller  $\sigma$  value will indicate a more severity degree of the cavitation. The cavitation number is calculated as

$$\sigma = \frac{p_{in} - p_v}{0.5\rho V_0^2}, \quad (23)$$

where  $p_{in}$  is the pressure at the inlet;  $p_v$  is the saturated vapor pressure of the medium at ambient temperature and  $p_v = 3167$  Pa in this study;  $\rho$  is the density of the medium;  $V_0$  is the flow rate of the medium.

In the Fluent software, by adjusting the inlet pressure, different cavitation conditions can be simulated. For transient simulations, the flow field snapshots are captured at various time intervals and exported as the Tecplot files. These files are then processed by the proposed DMD method using a MATLAB program. In this study, an inlet pressure of 9000 Pa is chosen to achieve the targeted cavitation conditions.

### 4.1. Modal decomposition results

Based on the analysis in Section 3.4, the transient time step for this study is  $dt = 2.78 \cdot 10^{-4}$  s, with 167 distinct flow snapshots collected over time. These snapshots are processed using the proposed DMD method, resulting in 166 reduced-order modes. The eigenvalues are of great significance in characterizing the stability of the flow field. Figure 4 shows the distribution of the eigenvalues of the flow field, where the real axis indicates the fundamental part of the eigenvalues, and the dashed axis is the imaginary part of the eigenvalues. It can be seen that the eigenvalues are symmetric along the real axis, which indicates that the eigenvalues are expressed as a conjugate pair whose modulus can be used to represent the stability of the flow field. It can also be noted that most of the points of the eigenvalues are distributed in the unit circle of the dashed line, indicating that the modes of the flow field in the pump are in periodic or stable conditions.

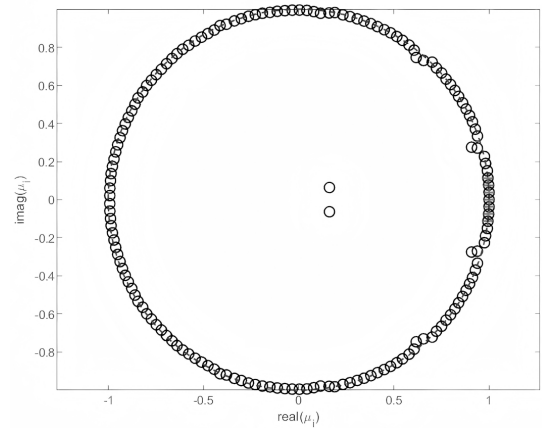


Fig. 4. Distribution of eigenvalues of the flow field

Since  $\tilde{A}$  is a similar transformation of  $A$ ,  $\tilde{A}$  contains the main eigenvalues of  $A$ . Defining  $g_i$  as the growth rate and the frequency  $\omega_i$ , the following relationship can be obtained:

$$g_i = \text{Re}\{\log(\mu_i)\}/\Delta t, \quad (24)$$

$$\omega_i = \text{Im}\{\log(\mu_i)\}/\Delta t, \quad (25)$$

where  $\mu_i$  is the feature value and  $\Delta t$  is the time interval for each snapshot.

Figure 5 demonstrates the relationship between the growth rates and frequency distributions of the DMD modes, in which most of the decay rates are non-positive, and almost all of them appear in the form of conjugate modes (i.e., the energies are equal and the decay rates are also the same). If the modes with higher energy have a high decay rate, it is caused by two main reasons. The first one is that the modes with higher decay rates lose their energy and decay rapidly. The oscillations of these modes may be more pronounced at the initial moment but disappear quickly.

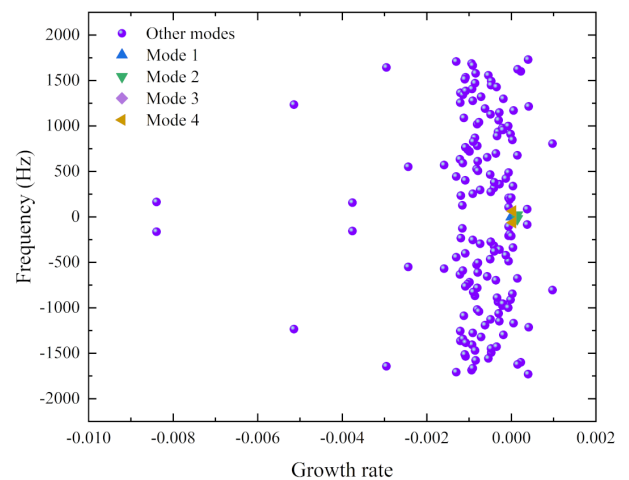


Fig. 5. Growth rate and frequency distribution of modes

The second reason is the pseudo-modes generated by errors due to numerical calculation or truncation errors in the DMD

simulations. When performing fluid simulations using finite difference, finite volume, or finite element methods, the errors due to spatial and temporal discretization may introduce pseudo-modes. When performing the SVD, it is often necessary to truncate small singular values to reduce the dimensionality and computational complexity of the data. This truncation process may lose some important information and lead to pseudo-modality. Pseudo-mode existence is a common problem in numerical simulation and DMD analysis. Through careful modal analysis and numerical optimization, the pseudo-modes can be effectively identified and dealt with to ensure the accuracy and physical significance of the DMD results.

Figure 6 illustrates the relationship between the frequency and energy of each mode. It can be seen that the frequency of the first-order modes is 0 Hz, which indicates that the modes are static or steady state modes of the system, and the modes do not oscillate in time, reflecting the basic equilibrium state of the system or the constant state under the initial conditions. Figure 7 shows the ratio of the first fifty orders to the total energy, where the first-order modes account for 53.5% of the total energy of all modes, reflecting that subsequent modes of each order are conjugate modes.

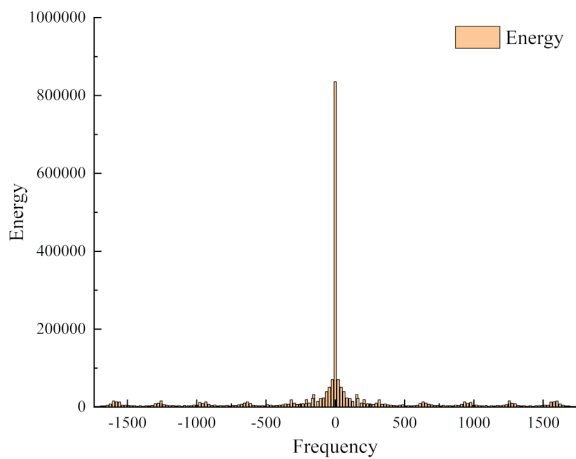


Fig. 6. Relationship between frequency and energy for each mode

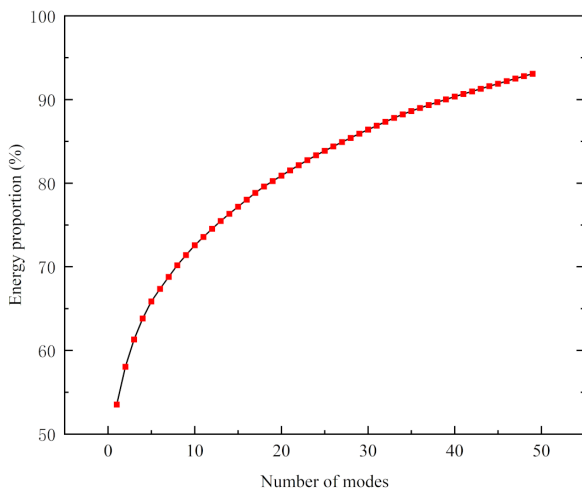


Fig. 7. Energy proportion of the first 50 orders

#### 4.2. Flow field cavitation

As Schmid [31] pointed out, a small number of modes often account for the majority of a system dynamic behaviour. The essence of the modal analysis is to simplify the examination of complex systems by isolating a few key modes. Although these modes may not represent the full information of the system, they still provide enough information to support engineering design and optimization. In practical engineering applications, such as the design and optimization of centrifugal pumps, the primary focus is on understanding the dynamic behaviour of the flow field and its effects on equipment performance. That is, in this study the first four modes of the pump may capture the main dynamic characteristics of the flow field. As a result, they offer critical insights that are essential for optimizing equipment performance and diagnosing potential faults [32]. For these reasons, detailed analysis is performed on the first four modes.

The first four orders of the flow field of the centrifugal pump cavitation are extracted, as shown in Fig. 8; and Fig. 9 depicts the velocity of the flow field without modal order reduction. Comparing Fig. 8 with Fig. 9, it is clear that the 1st-order mode (model 1) contains the vast majority of the energy of the flow field with stable and rich information about the original flow field.

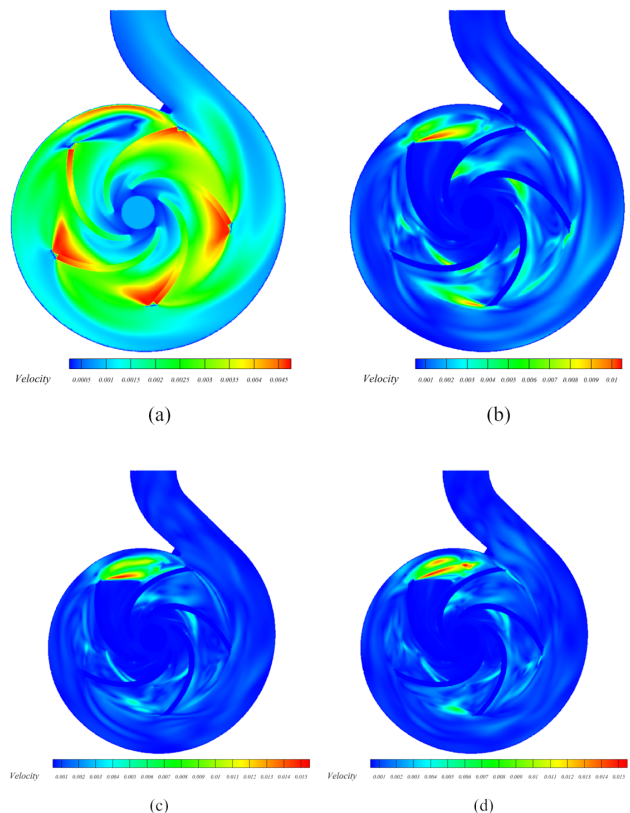


Fig. 8. Flow field for the first four orders of modes: (a) mode 1; (b) mode 2; (c) mode 3; (d) mode 4

In Fig. 8a, mode 1 represents the fundamental flow mode. This mode accounts for the largest proportion of energy of the original flow field as in Fig. 9 among all other modes and primarily

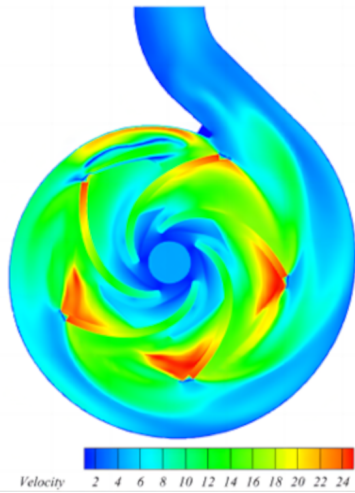


Fig. 9. Actual flow field of the centrifugal pump

reveals the flow field characteristics driven by the impeller blade geometry (because one can observe the blade profile in mode 1) and the flow attack angle. In essence, it represents the static distribution of the flow field in the context of unsteady flow, serves as the foundational framework for other dynamic modes, and provides key background information for the modal analysis.

In Fig. 8b, mode 2 corresponds to the impeller rotation frequency and highlights the significant impact of the interaction between the impeller rotation and the volute. Specifically, it reveals the flow separation and vortex formation caused by the pressure fluctuations when the impeller blade sweeps past the volute tongue. Under cavitation conditions, this dynamic-static interference exacerbates the development of the cavitation, leading to periodic cavitation regions on the blade suction side. From the perspective of the cavitating flow, mode 2 may also capture the periodic pressure fluctuations caused by the formation and collapse of the cavitation bubbles. These fluctuations induce the flow separation and vortex shedding on the blade suction side, further complicating the flow structure. Throughout one impeller rotation cycle, alternating high-energy fluid clusters continuously form on the blade suction side. As these clusters move downstream, they gradually stretch and diffuse to ultimately generate a wake at the impeller outlet. This behaviour is captured by mode 2, which characterizes the flow disturbances induced by the interaction between the impeller and the volute.

When the centrifugal pump operates under the cavitating conditions, mode 3 and mode 4 reveal the higher-order dynamic flow features. In Fig. 8c, mode 3 uncovers the formation of small-scale cavitation vortices on the blade suction side. These vortices evolve, stretch, and shed as the impeller rotates, with their development closely linked to the periodic growth and collapse of the cavitation bubbles. This process generates pressure fluctuations on the blade surface and complex flow separation phenomena.

In Fig. 8d, mode 4 further captures the rapid evolution and dissipation of even smaller and higher-frequency cavitation vortices, which are closely associated with the high-frequency os-

cillation, collapse, and regeneration of the cavitation bubbles. It leads to high-frequency pressure pulses and more complex flow separation behaviours in the local flow field. It can be noted that mode 3 and mode 4 provide valuable insight into the separation and shedding of the unstable vortex structures on the blade suction side, driven by the interaction between the impeller rotation and the volute in cavitating the centrifugal pump flow. These higher-order modes represent the dynamic-static interference harmonics and reveal the intricate dynamic characteristics of the cavitation flows.

Following the reduction and reconstruction of the flow field using the proposed DMD, a loss function is employed to evaluate the relationship between the reduction and reconstruction. The loss function is expressed as

$$\text{Loss} = \frac{\|X_1^{N-1} - \Phi D_\alpha V_{\text{and}}\|_F}{\|X_1^{N-1}\|_F} \times 100\%. \quad (26)$$

After sorting the DMD amplitudes obtained from the surface in order of magnitude, the velocity field reconstructed at arbitrary point in time has been obtained as

$$v_i^{\text{rec}} = \sum_{i=1}^{N-1} \varphi_i (\mu_i)^{i-1} \alpha_i. \quad (27)$$

According to equation (27) and the numerical simulation results, the error of reconstructing the flow field at an arbitrary moment can be obtained as

$$\text{Rec}_i = \frac{\|v_i^{\text{CFD}} - v_i^{\text{rec}}\|_2}{\|v_i^{\text{CFD}}\|_2} \times 100\%, \quad (28)$$

where  $v_i^{\text{CFD}}$  is the velocity field at moment  $i$  obtained by the CFD simulation and  $\text{Rec}_i$  is the error between the reconstructed flow field and the CFD flow field.

Figure 10 shows the error plot of the original flow field of the centrifugal pump and the flow field after the order reduction. The figure shows that with the increase in the number of modes, the error between the reconstructed cavitation flow field and the original flow field shows a decreasing trend. The modal loss decreases gradually, and when the modes reach the 100th order, the error of the downgraded flow field compared with the original flow field is 3.2%. Meanwhile, the first mode already contains most of the information of the flow field, and the error of the first order mode is 19.2%; the error of the first four modes is 14.2%. These results indicate that increasing the number of modes over a smaller range of modal numbers does not significantly improve the reconstruction accuracy. The cavitation flow field of the centrifugal pump is a highly nonlinear physical field with a complex turbulent structure, and the flow instability caused by the formation and disappearance of the cavitation bubbles is more prominent, especially under the cavitation conditions. The calculation of losses is obtained by comparing the actual and reconstructed flow fields for each time series, and the modes are chosen based on the total energy of the flow field. It is found that increasing the number of modes is not that effective

in reducing the error because the temporal fluctuations of the flow field itself may increase the error. Only when the number of modes is large enough it is possible to eliminate the errors caused by inconsistencies in the loss calculation.

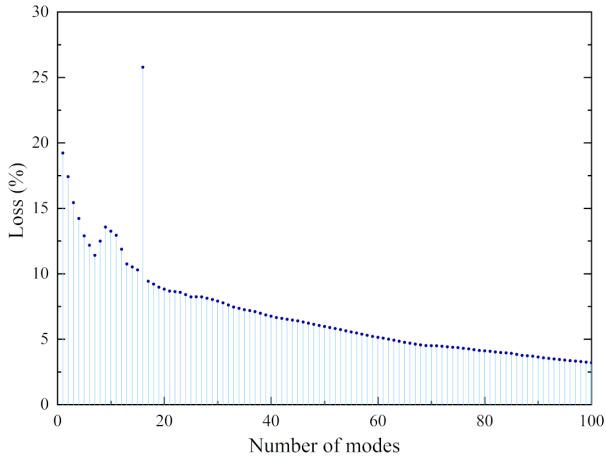


Fig. 10. Loss plot: order-reduction flow field vs. original flow field

### 4.3. Flow field reconstruction

The order-reduction flow field is extracted from the original flow field data, and the flow field reconstruction is given in Fig. 11. Figure 12 shows the error plot of the reconstructed flow field over the original flow field. From the error curve, it can be seen that the reconstruction error can eventually be reduced to less than 5% in one cycle, and the reconstructed flow field is not much different from the original flow field. Therefore, the reconstructed flow field is accurate.

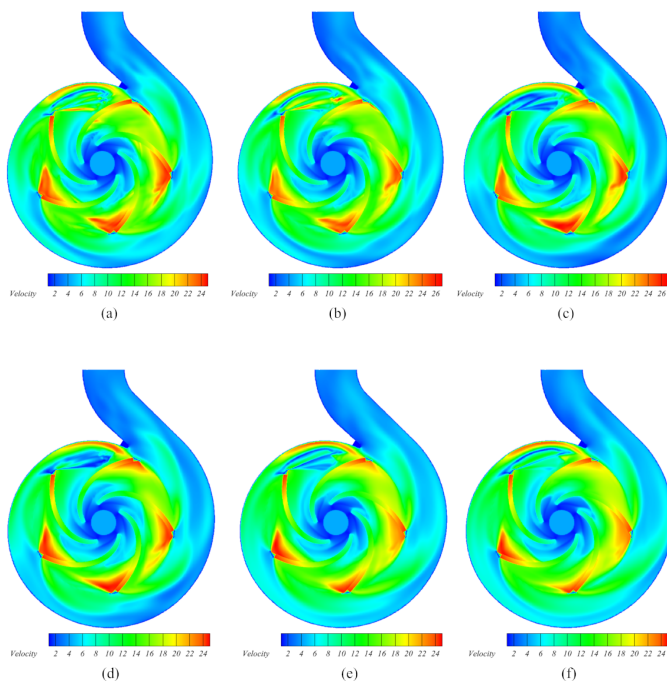


Fig. 11. Reconstructing the flow field: (a) reconstruction 1; (b) reconstruction 2; (c) reconstruction 3; (d) reconstruction 4; (e) reconstruction 5; (f) reconstruction 6

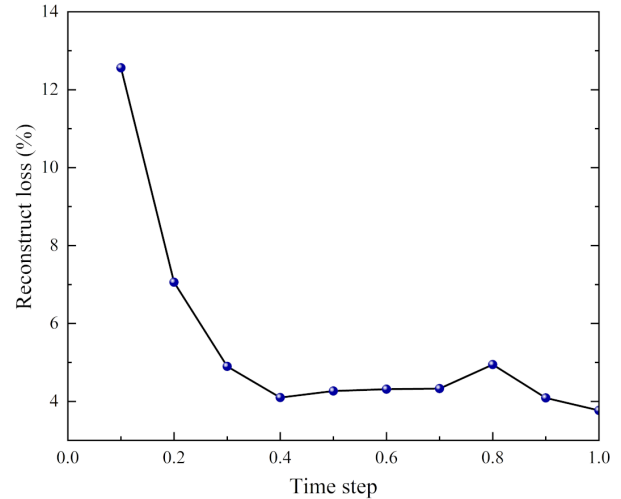


Fig. 12. Error curves between the reconstructed and original flow fields

## 5. CONCLUSIONS

This paper investigates the rapid order reduction of the flow field of a centrifugal pump under the cavitation state based on the dynamic mode decomposition method of singular value decomposition. The mode decomposition and flow field reconstruction of the centrifugal pump flow field are completed through the in-depth analysis and discussion of the eigenvalues of the modes, the frequencies, the energies of the modes in each order, and the attenuation rates. The reconstruction results show that the error between the reconstructed flow field and the original flow field is less than 5%, and it can correctly reflect the flow field. The main conclusions we obtained are as follows:

1. The dynamic mode decomposition (DMD) method based on singular value decomposition (SVD) accurately captures the modal information of the flow field under the cavitation condition of the centrifugal pump, extracting the frequency variations within the flow field. The flow field in the pump is periodic or stable, and the first-order modes are time-averaged modes, which contain most of the energy of the flow field and reflect the characteristics of the time-averaged flow field.
2. The DMD method can significantly reduce the order reduction time for flow-field analysis and quickly capture the main features of the flow field. Detailed analysis, prediction, and flow field reconstruction can be accomplished in just a few tens of seconds using the DMD method. In addition, DMD can effectively identify the core dynamic modes in the system behaviour, which is especially critical for dealing with complex flow fields such as cavitation. This modal identification technique not only simplifies the model structure but also reduces the processing time from tens or even hundreds of hours to a much shorter time window than the traditional CFD analysis while ensuring accuracy, thus significantly saving the computational cost and improving the analysis efficiency.
3. The DMD proves to be an effective tool for the rapid dimensionality reduction of the cavitation flow field in the centrifugal pumps. The error between the original and reduced-

order flow fields can be reduced to below 3.2%, indicating that the reduction process preserves sufficient key characteristics of the flow field. Furthermore, the error between the order-reduced flow field and the original flow field remains within approximately 5%, suggesting that the predicted flow closely matches the characteristics of the pump flow field. As a result, the proposed DMD method not only enables efficient dimensionality reduction for the centrifugal pumps but also facilitates accurate flow field reconstruction under the cavitating conditions.

One limitation of the current research lies in that the two-dimensional (2D) model is used for the flow field reconstruction. The next study will extend the 2D model to a 3D one to describe more details of the flow field. The research outcome will provide an effective tool for flow field modal analysis, rapid order reduction, and modal reconstruction for the centrifugal pumps under cavitation conditions.

## ACKNOWLEDGEMENTS

The authors would like to thank the reviewers for their constructive comments and suggestions.

## DATA AVAILABILITY

Data will be made available on request.

## CREDIT AUTHORSHIP CONTRIBUTION STATEMENT

Y. Zhang and L. Zhang performed the formal analysis and wrote the manuscript text; Y. Zhang and T. Sun prepared the data, methodology, and software; T. Sun and C. Wang analyzed the data; D. Jiang and Z. Li proposed the conceptualization and performed the supervision and funding acquisition; Z. Li reviewed and edited the manuscript text.

## REFERENCES

- [1] J. Černetič, "The use of noise and vibration signals for detecting cavitation in kinetic pumps," *Proc. Inst. Mech. Eng -Part C-J. Mech. Eng. Sci.*, vol. 223, no. 7, pp. 1645–1655, 2009.
- [2] J.P. Franc and J.-M. Michel, *Fundamentals of cavitation*. Springer science & Business media, 2006.
- [3] R. Tao, R. Xiao, F. Wang, and W. Liu, "Cavitation behavior study in the pump mode of a reversible pump-turbine," *Renew. Energy*, vol. 125, pp. 655–667, 2018.
- [4] R. Knapp, J. Daily, and F. Hammit, *Cavitation*. McGraw-Hill Book Company: New ork, 1970.
- [5] R.B. Medvitz, R.F. Kunz, D.A. Boger, J.W. Lindau, A.M. Yocum, and L.L. Pauley, "Performance analysis of cavitating flow in centrifugal pumps using multiphase CFD," *J. Fluids Eng.*, vol. 124, no. 2, pp. 377–383, 2002.
- [6] A.R. Al-Obaidi, "Experimental diagnostic of cavitation flow in the centrifugal pump under various impeller speeds based on acoustic analysis method," *Arch. Acoust.*, vol. 48, no. 3, pp. 159–170, 2023.
- [7] F. Orlandi, L. Montorsi, and M. Milani, "Cavitation analysis through CFD in industrial pumps: A review," *Int. J. Thermofluids*, vol. 20, p. 100506, 2023.
- [8] Y. Li, G. Feng, X. Li, Q. Si, and Z. Zhu, "An experimental study on the cavitation vibration characteristics of a centrifugal pump at normal flow rate," *J. Mech. Sci. Technol.*, vol. 32, pp. 4711–4720, 2018.
- [9] H.K. Sakran, M.S. Abdul Aziz, M. Abdullah, and C. Khor, "Effects of blade number on the centrifugal pump performance: a review," *Arab. J. Sci. Eng.*, vol. 47, no. 7, pp. 7945–7961, 2022.
- [10] Z. Wei, Y. Tang, L. Chen, H. Zhang, and F. Li, "Fast prediction of the performance of the centrifugal pump based on reduced-order model," *Energy Rep.*, vol. 9, pp. 51–64, 2023.
- [11] W. Zhang, L. Hu, H. Li, B. Zhu, and F. Wang, "Numerical analysis of bubble size effect in a gas-liquid two-phase rotodynamic pump by using a bubble coalescence and collapse model," *Chem. Eng. Res. Des.*, vol. 191, pp. 617–629, 2023.
- [12] Z. An, L. Zhounian, W. Peng, C. Linlin, and W. Dazhuan, "Multi-objective optimization of a low specific speed centrifugal pump using an evolutionary algorithm," *Eng. Optim.*, vol. 48, no. 7, pp. 1251–1274, 2016.
- [13] R. Hirschi, P. Dupont, F. Avellan, J.-N. Favre, J.-F. Guelich, and E. Parkinson, "Centrifugal pump performance drop due to leading edge cavitation: numerical predictions compared with model tests," *J. Fluids Eng.*, vol. 120, pp. 705–711, 1998.
- [14] G. Li *et al.*, "Liquid-vapor two-phase flow in centrifugal pump: Cavitation, mass transfer, and impeller structure optimization," *Vacuum*, vol. 201, p. 111102, 2022.
- [15] P.J. Schmid, "Application of the dynamic mode decomposition to experimental data," *Exp. Fluids*, vol. 50, pp. 1123–1130, 2011.
- [16] P.J. Schmid, L. Li, M.P. Juniper, and O. Pust, "Applications of the dynamic mode decomposition," *Theor. Computat. Fluid Dyn.*, vol. 25, pp. 249–259, 2011.
- [17] E. Alenius, "Mode switching in a thick orifice jet, an LES and dynamic mode decomposition approach," *Comput. Fluids*, vol. 90, pp. 101–112, 2014.
- [18] N. Vinha, F. Meseguer-Garrido, J. De Vicente, and E. Valero, "A dynamic mode decomposition of the saturation process in the open cavity flow," *Aerosp. Sci. Technol.*, vol. 52, pp. 198–206, 2016.
- [19] B.R. Noack, W. Stankiewicz, M. Morzyński, and P.J. Schmid, "Recursive dynamic mode decomposition of transient and post-transient wake flows," *J. Fluid Mech.*, vol. 809, pp. 843–872, 2016.
- [20] C. Pan, D. Xue, and J. Wang, "On the accuracy of dynamic mode decomposition in estimating instability of wave packet," *Exp. Fluids*, vol. 56, pp. 1–15, 2015.
- [21] W. Liang, T. Chen, G. Wang, and B. Huang, "Investigation of unsteady liquid nitrogen cavitating flows with special emphasis on the vortex structures using mode decomposition methods," *Int. J. Heat. Mass Transf.*, vol. 157, p. 119880, 2020.
- [22] Y. Xu, M. Peng, A. Cammi, C. Introini, and G. Xia, "Model order reduction of a once-through steam generator via dynamic mode decomposition," *Ann. Nucl. Energy*, vol. 201, p. 110457, 2024.
- [23] Y. Zhi, R. Qiu, R. Huang, and Y. Wang, "Dynamic mode decomposition and reconstruction of the transient propeller wake under a light loading condition," *Ocean Eng.*, vol. 269, p. 113532, 2023.

Y. Zhang, L. Zhang, C. Wang, T. Sun, Z. Li, and D. Jiang

- [24] Y. Liu, Q. Wu, B. Huang, H. Zhang, W. Liang, and G. Wang, "Decomposition of unsteady sheet/cloud cavitation dynamics in fluid-structure interaction via POD and DMD methods," *Int. J. Multiph. Flow*, vol. 142, p. 103690, 2021.
- [25] M. Liu, L. Tan, and S. Cao, "Dynamic mode decomposition of gas-liquid flow in a rotodynamic multiphase pump," *Renew. Energy*, vol. 139, pp. 1159–1175, 2019.
- [26] Y. Han and L. Tan, "Dynamic mode decomposition and reconstruction of tip leakage vortex in a mixed flow pump as turbine at pump mode," *Renew. Energy*, vol. 155, pp. 725–734, 2020.
- [27] J. Wang *et al.*, "Analysis of the flow field characterization on the cavitation water jet applied to planar and curved surfaces," *Phys. Fluids*, vol. 36, no. 10, 2024.
- [28] W. Wu, Y. Xu, Y. Yan, S. Li, J. Zhang, and Z. Wang, "Investigation on The Flow Characteristics of Rotating Nozzle Cavitation Water Jet Flow Field," *J. Appl. Fluid Mech.*, vol. 17, no. 12, pp. 2637–2651, 2024.
- [29] K. Yamamoto and Y. Tsujimoto, "A backflow vortex cavitation and its effects on cavitation instabilities," *Int. J. Fluid Mach. Syst.*, vol. 2, no. '1, pp. 40–54, 2009.
- [30] C. Dai, S. Hu, Y. Zhang, Z. Chen, and L. Dong, "Cavitation state identification of centrifugal pump based on CEEMD-DRSN," *Nucl. Eng. Technol.*, vol. 55, no. 4, pp. 1507–1517, 2023.
- [31] P.J. Schmid, "Dynamic mode decomposition of numerical and experimental data," *J. Fluid Mech.*, vol. 656, pp. 5–28, 2010.
- [32] P. Zhang, J. Pan, and F. Feng, "Modal Decomposition and Re-configuration of Gas-Liquid Two-Phase Unsteady Flow in A Centrifugal Pump by DMD," *Chin. J. Hydrodyn.*, vol. 38, pp. 808–817, 2023.